Time-Resolved Two-Dimensional Small Angle X-ray Scattering Studies of Oriented Poly (ethylene terephthalate)(PET) Using Paracrystalline Modeling Techniques

5 AUTHORS, INCLUDING:

Rob Rule
Ceramex Ltd
13 PUBLICATIONS **167** CITATIONS

SEE PROFILE

Arumugam Mahendrasingam
Keele University
81 PUBLICATIONS **1,156** CITATIONS

SEE PROFILE

Chelsea Martin
Columbia University
88 PUBLICATIONS **1,397** CITATIONS

SEE PROFILE

Time-Resolved Two-Dimensional Small Angle X-ray Scattering Studies of Oriented Poly(ethylene terephthalate) (PET) Using Paracrystalline Modeling Techniques

R. J. Rule,*,† D. H. MacKerron,‡ A. Mahendrasingam,§ C. Martin,§ and T. M. W. Nye†

ICI Chemicals and Polymers, Runcorn Technical Centre, P.O. Box 8, The Heath, Runcorn WA7 4QD, U.K., ICI Films R&T, Materials Research Centre, Wilton, Middlesborough, Cleveland TS6 8JE, U.K., and Department of Physics, University of Keele, Staffordshire ST5 5BG, U.K.

ABSTRACT: A paracrystalline macrolattice model has been used to provide a detailed description of the morphological changes which occur during the annealing of an oriented polyester, poly(ethylene terephthalate) (PET) at temperatures between 100 and 200 °C. The model structures were obtained by fitting the observed and calculated SAXS patterns using an automated series of computational routines. Accurate pictures of the paracrystalline structures, which have been generated according to the precise values of the model parameters, were able to provide a quantitative insight into the growth of the crystallites during the annealing process. The limitations of using a two-phase model with cylindrical symmetry to describe the structure of PET film are discussed.

1. Introduction

Two-dimensional small angle X-ray scattering (SAXS) is a tool which is commonly used in the investigation of the structure of oriented, semicrystalline polymers. The SAXS patterns obtained from these materials often consist of two broad meridional scattering features situated above and below the equator of the 2D image; these features arise from the periodic arrangement of crystals along the preferred direction of orientation in the sample. If the crystals in the sample have been sheared or rotated in some way such that two preferred orientations exist, then a so-called "four-point" pattern may be observed. A simple summary of the characteristic SAXS patterns which are obtained from typical, oriented polymer structures is provided[1] in Figure 1.

It is clear that an immediate, qualitative impression of the width and orientation of the crystallites may be gained by direct inspection of the pattern. However, it is also evident that gross structural differences often give rise to quite subtle changes in the appearance of the meridional scattering features.

The majority of the quantitative, structural studies which have investigated two-dimensional SAXS patterns from oriented semicrystalline polymers have been based on the paracrystalline theory of Hosemann et al.[2,3] The paracrystal model consists of a three-dimensional arrangement of crystallites which are located on the points of a disordered macrolattice (or superlattice). By variation of the size, separation, ordering, and orientation of these crystallites, highly diverse superstructures may be generated, which provide useful models for the morphology of oriented polymers.

Several materials have been studied using this approach and include linear polyethylene,[4,5] isotactic polypropylene,[6,7] and isotactic polybutene.[8] In many of these early works, the intensity profiles along certain
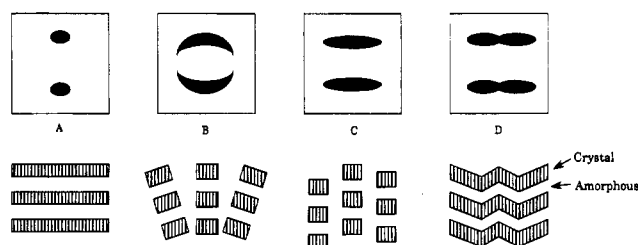
Figure 1. Commonly observed 2D SAXS patterns from typical oriented polymer structures (based on Rober et al.[1]).

sections of the two-dimensional pattern were analyzed to yield information on the polymer superstructure. More recently, a three-dimensional monoclinic paracrystalline macrolattice model has been developed by Wilke et al.[9-14] which has been used to calculate the entire two-dimensional SAXS intensity distribution for fitting to experimental patterns of polyethylene. In one particular form of this model, which is considered in this paper, the scattering units (or individual crystallites) are represented by identical cylinders. This paracrystalline approach has also been used to study the swelling of Nylon fiber[15] and has been modified to incorporate inclined lamellar structures in order to characterize more accurately SAXS patterns which possess a four-point character.[16]

Vonk[17] provided an alternative approach to the analysis of the complete two-dimensional scattering pattern by using the correlation function technique.[18] Attempts have also been made to calculate two-dimensional SAXS patterns on the basis of a model possessing alternating lamellar phases with an orientation distribution.[19,20] This model is formulated on the concept that the scattering arises from positive and negative deviations from the average density of the system whereas the calculations of the paracrystal theory are based on the excess density between crystal and amorphous regions.

In this paper, we report the application of the three-dimensional paracrystalline macrolattice model[9-14] to study the development of the semicrystalline structure of oriented poly(ethylene terephthalate) (PET) at various temperatures using time-resolved synchrotron SAXS. A simple, one-dimensional paracrystalline model ap-

* Author for correspondence. Tel: 44 - 01928 511437. FAX: 44 - 01928 581178. e-mail: rjr@dl.ac.uk.
† ICI Chemicals and Polymers.
‡ ICI Films R&T.
§ University of Keele.
® Abstract published in *Advance ACS Abstracts,* November 1, 1995.

proach has been used recently[21] to characterize SAXS patterns from PET fibers, although fits were only provided for equatorial and meridional slices of the 2D SAXS data. Several studies of the development of semicrystalline structure in oriented PET have been performed (see ref 22 and papers therein), although many of these investigations have involved a semiquantitative, ex-situ diffraction analysis of samples which have been annealed in oil. In this work, the high intensity of the synchrotron source is exploited to perform SAXS measurements in-situ on uniaxially oriented film from PET during an annealing program and the resulting 2D patterns are modeled conveniently using a self-converging routine.[23]

2. Theory

The complete theoretical description of the monoclinic paracrystalline macrolattice model is provided elsewhere.[9-14] In the model, it is assumed that the basic scattering unit is a cluster of cylinders which possess a stuctural perpendicular, **n**. Each cluster is assumed to exhibit rotational symmetry about the overall orientation direction. The general intensity formula for such a model is given by[14]

$$I(r^*, \theta^*) = \sum_{n=0} [2/(4n + 1)] D_{2n} G°_{2n}(r^*) P_{2n}(\cos \theta^*) \quad (1)$$

where

$$D_{2n} = [(4n + 1)/2] \int_0^\pi d\alpha \sin \alpha \, D(\alpha) \, P_{2n}(\cos \alpha) \quad (2)$$

$$G°_{2n}(r^*) =$$
$$[(4n + 1)/2] \int_0^\pi d\theta^* \sin \theta^* \int_0^{2\pi} d\varphi^* \{I_1(\mathbf{b}) \, P_{2n}(\cos \theta^*)\} \quad (3)$$

r^*, θ^* and φ^* are spherical coordinates in reciprocal space, P_{2n} are Legendre polynomials, and $I(r^*, \theta^*)$ represents the intensity at the point (r^*, θ^*) in the plane of the area detector. The magnitude of the scattering vector, $|\mathbf{b}|$, is given by $2(\sin \theta)/\lambda$, where 2θ is the scattering angle and λ is the X-ray wavelength (in this case $\mathbf{b} = \mathbf{q}/2\pi$).

The term D_{2n} contains the orientation distribution of the structure and takes the form of a Gaussian of width σ. The term $I_1(\mathbf{b})$ represents the scattering intensity of a basic unit (or cluster) and is given by

$$I_1(\mathbf{b}) = |F(\mathbf{b})|^2 Z(\mathbf{b}) \quad (4)$$

with $F(\mathbf{b})$ the form factor of a single crystallite (cylinder) and $Z(\mathbf{b})$ the lattice factor of the ideal monoclinic paracrystalline macrolattice.

The complete structure is governed by several parameters (which are described in greater detail elsewhere[9-14]): the cylinder dimensions, H and D; the macrolattice dimensions, a_3 and a_r; the relative disorder parameters, g_r, g_3 and g_{33}, the monoclinic macrolattice angle, β; the centre of the orientation distribution, α_0, and its width, σ. The model allows for enormous flexibility in generating highly diverse structures and in calculating and fitting various SAXS intensity features.

The model assumes that each cluster has rotational symmetry about its structural perpendicular (**n**) and that the distribution of the structure perpendiculars has
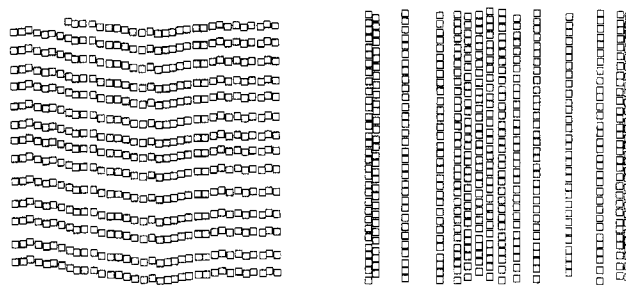
Figure 2. Paracrystalline arrangements of cylinders to give lamellar and fibrillar morphologies (based on Wilke et al.[14]).

rotational symmetry about the overall orientation direction (**f**). The model also assumes that the individual cylinders (often identified as crystallites) are identical in size and have sharp boundaries. Naturally, both of these assumptions are physically unrealistic, but the model is still capable of providing useful representations of the structure of oriented polymers. For example, lamellar and fibrillar morphologies may be generated by an appropriate choice of model parameters (see Figure 2).

3. Experimental Section

Diffraction Measurements. SAXS experiments were performed using station 2.1 at the Synchrotron Radiation Source, Daresbury Laboratory, Warrington, U.K. This station[24] possesses a Ge(111) triangular monochromator with a 10.5° symmetric cut along with a 70 cm cylindrically-bent, fused-quartz mirror, producing a vertically focused beam with a flux of around 10^{12} photon/s at a wavelength of 1.54 Å. The scattering patterns were collected using a gas-filled, multiwire area detector located behind the sample in a simple transmission geometry with the plane of the detector normal to the incident beam direction. The sample-to-detector distance used for the majority of the experiments was around 2.5 m, giving a measurable q-range of 0.014–0.18 Å^{-1}. The raw SAXS patterns were normalized to account for the variations in incident beam flux and exposure time using an ionization chamber located after the sample. Corrections were also made to account for the nonuniformity of response of the individual detector elements (using radiation from a ^{55}Fe source) and the intrinsic spatial distortion of the image (using a square grid mask).

The apparatus used for the constrained annealing experiments consisted of an X-ray camera[25] designed and constructed at the University of Keele, U.K. The camera comprises an oven containing two 800 W heaters and recirculating fans which control air temperature to within ±1 deg. In addition, the camera is equipped with a bidirectional drawing apparatus (which is driven by two stepper motors and controlled by portable PC) and a strain gauge.

The annealing study was performed on a sample of film from PET which had been prepared and stretched uniaxially using a small scale film production process. The film was produced with a draw ratio of 3.3:1 and had a final thickness of 240 μm. From this film, two specimens of width 40 mm and length 100 mm were cut, superimposed, and mounted in the X-ray camera such that the draw direction in the film was restrained between clamps and the beam impinged normal to the plane of the film. A SAXS pattern was recorded at room temperature using an exposure time of 3 min and the sample then heated stepwise, under restraint, to temperatures of 100, 140, 160, 180, and 200 °C. A SAXS pattern was recorded at each temperature under isothermal conditions, immediately after thermal equilibrium had been achieved. The temperature of the sample was measured using a Chrome-Alumel thermocouple which was in intimate contact with the film. In the final stage of the thermal program, the sample was cooled to room temperature and a further SAXS pattern recorded.

4. Results

The oriented sample of PET gave a featureless SAXS pattern at room temperature, suggesting that the level of crystallinity was rather low. During heating, the sample crystallized and broad, discrete meridional scattering maxima developed, corresponding to an ordered semicrystalline structure in which the crystallites had adopted the preferred orientation of the sample. At higher temperatures, the scattering features became sharper and narrower, suggesting a lateral growth of the crystallites and increasing order along the orientation direction.

The SAXS patterns (each consisting of 512 × 512 pixels of data) were corrected for experimental artefacts and attempts were made to simulate the scattering features using two-dimensional intensity functions calculated according to the paracrystalline macrolattice model. In order to reduce the simulation to a more manageable size, the original patterns were reduced to 256 data points by taking an averaged selection of data points to form a unique quadrant of the image. In addition to reducing the size of the image, the procedure allowed an uncertainty value to be attached to each data point by comparing the intensity values in each of the four symmetry related quadrants of the experimental pattern (which possesses horizontal and vertical mirror symmetry). The standard deviation of these four values was taken as a rough measure of the uncertainty for each data point and served an extremely useful role in the fitting process.

The calculation of this reduced 16 × 16 image was found to be an acceptable compromise for fitting requirements since several hours were required to calculate a complete 512 × 512 image. Several data points surrounding the beamstop were also removed from the reduced image so that none of the parasitic scattering was included in the modeling process. The calculation of a reduced image took about 2 min (using a Silicon Graphics Iris machine).

The quality of the fit between the calculated and experimental images was provided by an error-weighted subtraction of the two patterns under comparison to give a standard χ^2 value, which was minimized during fitting:

$$\chi^2 = (1/N)\sum_{x=1}^{16}\sum_{y=1}^{16}\{[I_o(x,y) - I_c(x,y)]/I_e(x,y)\}^2 \quad (5)$$

where I_o is the observed intensity, I_c is the calculated intensity, I_e is the uncertainty, and $N = 16 \times 16$.

Several approaches were employed in order to obtain the best match between experimental and calculated SAXS patterns. The most straightforward approach involved incremental parameter fitting—varying each parameter in turn and accepting any improvements in χ^2. This process was rather problematic, since it frequently encountered local minima (which were not a good match to the experimental pattern) beyond which the fit could not proceed. The likelihood of obtaining the best match to the experimental pattern was improved significantly by searching through a database of several thousand similar patterns to select the best starting point for the fit.

A further method was devised in order to provide an efficient search of possible solutions. Its principle was similar to incremental parameter fitting but allowed a record to be kept of all encountered patterns. The fitting

proceeded along the path of most rapid improvement in χ^2 by fixed parameter increments until a (local) minimum was encountered. The position of the local minimum was stored (in terms of the model parameters and χ^2), and a new starting point was selected with a higher χ^2. As such, the process provided a comprehensive search of many thousands of solutions similar to the experimental pattern, irrespective of whether or not they improved the fit. In addition, the stored positions of the local minima could be used to assess the variation of χ^2 with any individual parameter in the model.

These three fitting methods were combined in an automatic routine to obtain the best match between calculated and experimental patterns. At the end of the fitting process, a full scale image was calculated for each pattern using the parameters obtained for the best fit to the reduced image. Adequate fits were obtained for all of the observed SAXS patterns (other than the featureless room temperature pattern prior to annealing). In general, the χ^2 values obtained lay within the range 0.9–2.1. Interestingly, the diffuse pattern recorded at 100 °C provided a rather poor visual fit despite having the best χ^2 value (due to the high relative uncertainty associated with the weak intensity values). Figure 3 provides a comparison of four of the experimental and calculated SAXS patterns. The model parameters which correspond to each of the calculated patterns are provided in Table 1.

The structural changes during annealing are best appreciated in pictures of the model structure which were generated according to the precise values of the parameters obtained for the best fits. These pictures represent an accurate side view of a typical cluster of cylinders whose position and arrangement were simulated according to the cylinder size, the lattice dimensions, and the random disorder parameters of the model. No indication is provided of the degree of orientation of the clusters with respect to the overall orientation axis; this is a combination of the mean orientation (α_0) and the angular spread of the crystallites (a Gaussian distribution of width σ). In Figure 4 the model structures are illustrated for the PET sample after annealing at 100 and 200 °C.

It is clear from the results presented in Table 1, the structures depicted in Figure 4, and the graph shown in Figure 5 that both of the cylinder dimensions increase with increasing annealing temperature corresponding to the growth in the thickness and lateral dimensions of the crystallites in the sample. The values obtained for the crystallite size compare reasonably well with values quoted[21] for PET fibers annealed for several hours at 200 °C. An increase in the long period spacing (which is provided by the macrolattice parameter a_3) was also observed with increasing annealing temperature. This phenomenon is related not only to a reorganization of the structure during the growth of the crystals at higher temperatures but is also related to the effects of thermal expansion. In fact, it is interesting to note that the model structure obtained at room temperature after annealing was very similar to the final structure at 200 °C; the principal difference was the greater separation of the crystallites (cylinders) at 200 °C, which can be attributed to thermal expansion.

It is notable that, on initial inspection, none of the simulations of the model structures was strictly fibrillar or lamellar in appearance. However the variation of the lateral disorder parameter g_r, which decreased from 0.62 at 100 °C to around 0.1 at 200 °C, suggests that the
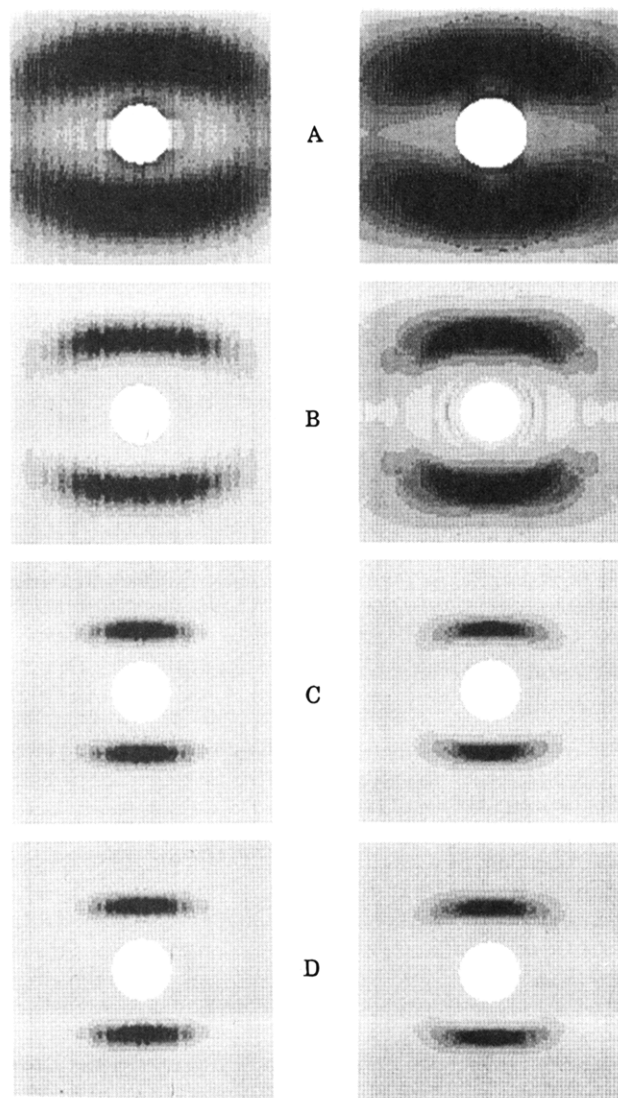
Figure 3. Comparison of experimental (left) and calculated (right) 2D SAXS patterns obtained from oriented PET film during annealing: (A) 100 °C; (B) 160 °C; (C) 200 °C; (D) 30 °C (postanneal).
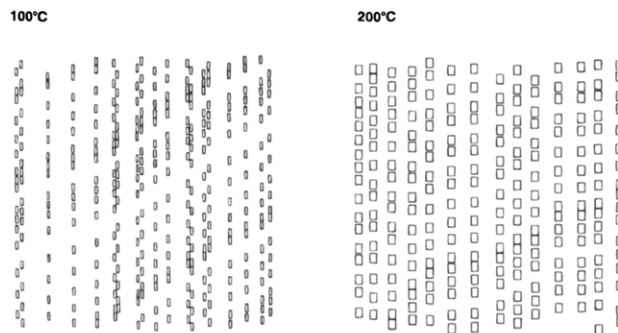

Figure 4. Predicted structure from SAXS patterns of oriented PET according to paracrystalline macrolattice model at 100 and 200 °C (the rectangles represent the side view of the cylinders in the model).

Figure 5. Graph of cylinder dimensions (obtained from the paracrystalline macrolattice model) versus annealing temperature for the oriented PET film.

Table 1. Model Parameters Obtained for the Best Fits to the Experimental SAXS Pattern from Annealed PET Samples

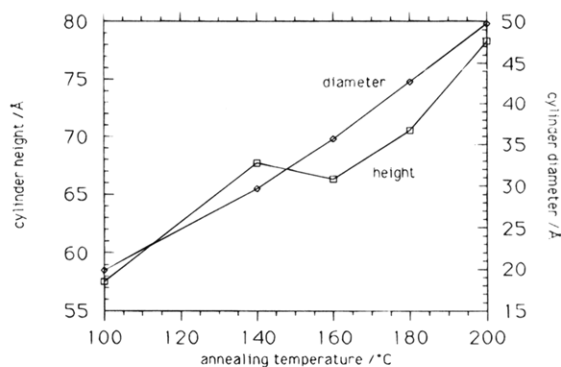|	annealing temp/°C					
	100	140	160	180	200	30 (postanneal)
H Å	58	68	66	71	78	75
D Å	20	30	36	43	50	52
a_3 Å	93	99	109	111	123	115
a_r Å	93	181	198	157	156	157
β/deg	59	58	71	61	55	54
g_{33}	0.38	0.22	0.22	0.22	0.20	0.20
g_r	0.67	0.08	0.11	0.07	0.12	0.09
g_3	0.04	0.27	0.21	0.38	0.36	0.39
σ/deg	16	17	13	14	14	11
α_0/deg	0	2	2	1	1	0

morphology is more stratified, or lamellar-like, after annealing at higher temperatures. In addition, the value of g_{33} decreased from 0.38 at 100 °C to 0.2 at 200 °C, implying that the degree of order along the orientation direction increases with increasing annealing temperature.

5. Discussion

Although the paracrystalline macrolattice model provides a fairly complex, quantitative interpretation of the structure of oriented semicrystalline polymers, it can be regarded only as a simple idealization of the sample morphology in the case of the PET film. The paracrystal model uses a straightforward two-phase description of the structure in which the boundaries between the phases are sharp and the crystallites are identical in size. It has been reported that the semicrystalline structure in PET is best described[26] in terms of three distinct components: the crystalline phase, the amorphous phase, and an intermediate, partially oriented phase. It has also been shown[11] that the introduction of a transition zone between crystal and amorphous domains in a paracrystalline lamellar model has a significant effect on the meridional scattering intensity for samples with high crystallinity. Thus it is reasonable to assume that a simple, two-phase model will not be able to reproduce perfectly the SAXS features observed for PET.

Modifications to the model are possible[14] to include such features as diffuse phase boundaries and a distribution of crystallite sizes but the calculations become even more cumbersome as the number of model parameters increases. The comparatively simple nature of the model used in this work will therefore limit the accuracy of its prediction. This is evident from the values of crystallinity which can be derived from the model parameters. In fact, the estimated values of the crystallinity at each annealing temperature according to the model were all rather low (<10%) although the trend of increasing crystallinity with increasing annealing temperature was correctly predicted.

In order to investigate in greater detail the low crystallinities predicted by the model, a one-dimensional correlation function[27-29] was calculated for the projection of the SAXS intensity onto the meridian of each of

Table 2. Morphological Parameters Obtained through Correlation Function Analysis (SAXS) and Scherrer Analysis (WAXS)

annealing temp/°C	SAXS correlation function analysis			WAXS Scherrer analysis cryst size /Å	
	cryst thickness/Å	D spacing/Å	ϕ_c	$\{1, 0, -5\}$	$\{010\}$
100	15	78	0.26		
140	27	88	0.31	55	31
160	30	94	0.32		
180	33	100	0.33		
200	39	110	0.35	68	55
postanneal (room temp)	38	105	0.36		

the patterns. The one-dimensional correlation function, which is essentially a Fourier transform of the projected SAXS intensity, provides a description of the variation in electron density in the direction of orientation within the sample. It is obtained from a transformation of the extrapolated SAXS profile, the extrapolation at high Q being performed using a damped Porod's law behavior to incorporate the effects of an interfacial layer.

This correlation function assumes that the sample possesses an ideal lamellar morphology with infinite crystalline lamellae lying with their planes perpendicular to the direction of orientation. Once more, this is a simplification of the oriented PET morphology but provides an alternative estimate of the dimensions of crystalline and amorphous domains along the orientation axis. The interpretation of the correlation function allows the direct evaluation of several structural parameters which describe the ideal lamellar morphology. These include the d spacing (or long period), the average thicknesses of the crystalline and amorphous layers, the (linear) crsytallinity, ϕ_c, the density difference between the two phases, and the thickness of the interfacial region between the phases.

Furthermore, estimates of the crystalline dimensions were also obtained using a standard Scherrer analysis of certain peaks from wide angle X-ray scattering. The Scherrer analysis was performed on the $\{1,0, -5\}$ and $\{010\}$ Bragg peaks to give dimensions which are analogous to the cylinder height and diameter (respectively) in the paracrystalline model.

The results of the correlation function analysis and Scherrer analysis are provided in Table 2. The linear crystallinities determined by the correlation function technique (26−36%) are much larger than those determined in the paracrystal model and are more consistent with expectations. However, the cylinder height in the paracrystal model is consistently larger than the crystal thickness determined using the correlation function. This discrepancy may be attributed to the transition zone which is included in the correlation function calculations but not in the paracrystal macrolattice model. As mentioned earlier, the effects of such a transition zone upon the SAXS intensity profile have been shown to be highly significant[11] and could be responsible for the diffferences between the crystallinities and crystallite thicknesses determined by these two techniques. Indeed, a recent study[30] of PET suggests that the presence of thick order−disorder interfacial layers can affect the accuracy of crystallinity measurements using SAXS.

Further comparison of the results presented in Table 2 with the paracrystal model results in Table 1 suggests that there is a close correspondence between the cylinder dimensions and the crystallite dimensions determined by the Scherrer analysis of the $\{1,0,-5\}$ and $\{010\}$ WAXS reflections (which correspond to the cylinder height and width, respectively).

In summary, it has been shown that the correlation function analysis of the SAXS patterns provides a more credible measurement of crystallinity in oriented PET than the paracrystal macrolattice model. However, the assumption of an ideal lamellar morphology is highly simplistic, particularly at lower annealing temperatures, for which the SAXS meridional spot is extremely broad and diffuse. The attempts to model the entire 2D SAXS pattern have failed to predict sensible crystallinity levels. However, the macrolattice model does provide crystallite dimensions which compare favorably with those determined using WAXS. The origin of the discrepancies between the correlation function approach and paracrystal results is not clearly understood but may be related to the effects of interfacial regions.

An additional concern involves the rotational symmetry which is an implicit assumption of the model but which may be absent in a film sample. As such, the structural features of the model will only be strictly relevant to the morphology in the plane of the film and the sample may possess a different structural arrangement through the thickness of the film. In such a case, it would be necessary to record separate SAXS patterns with the X-ray beam impinging parallel and perpendicular to the plane of the film in order to obtain a complete three-dimensional picture of its morphology.

Despite these limitations, the paracrystalline macrolattice model has been able to provide a useful, quantitative picture of the complex structural changes which occur during the crystallization and annealing of an oriented semicrystalline polymer. In addition, the pictures of the paracrystal morphology provide a useful visual impression of the size, arrangement and organization of the structural entities which give rise to the scattering features.

The paracrystal model has been used in an attempt to exploit the structural information contained in the entire 2D SAXS pattern, rather than limiting the analysis to selected one-dimensional slices of the image. The development of software based on the paracrystal model containing routines dedicated to the automatic fitting of observed SAXS pattern (using three successive methods) has now enabled the advantages of this model to be applied to the rapid interpretation of 2D SAXS patterns. This is of particular importance to time-resolved, in-situ scattering measurements, where a single experiment may yield many 2D patterns. In the future, the possibility of performing in-situ simultaneous wide angle and small angle 2D scattering measurements would provide further possibilities in determining the molecular arrangement as well as the size, orientation and ordering of the polymer crystallites on a length scale of 1−1000 Å.

to this work: D. J. Blundell, G. Eeckhaut, R. J. Oldman, R. Pendlebury (ICI), and W. Fuller (Keele University).

References and Notes

(1) Rober, S.; Bosecke, P.; Zachmann, H. G. *Makromol. Chem., Macromol. Symp.* **1988**, *15*, 295.

(2) Hosemann, R.; Bagchi, S. N. *Direct Analysis of Diffraction by Matter*; North-Holland: Amsterdam, 1962.

(3) Bonart, R.; Hosemann, R. *Kolloid Z. Z. Polym.* **1963**, *186*, 16.

(4) Cackovic, J. L.; Hosemann, R.; Cackovic, H. *Kolloid Z. Z. Polym.* **1971**, *247*, 824.

(5) Hosemann, R.; Cackovic, J. L.; Sassoui, M.; Weick, D. *Prog. Colloid Polym. Sci.* **1979**, *66*, 143.

(6) Cackovic, J. L.; Hosemann, R.; Cackovic, H.; Ferrero, A.; Ferracini, E. *Polymer*, **1976**, *17*, 303.

(7) Ferrero, A.; Ferracini, E.; Cackovic, J. L.; Cackovic, H. *J. Polym. Sci. Polym. Phys. Ed.* **1984**, *22*, 485.

(8) Ferracini, E.; Ferrero, A.; Cackovic, J. L.; Hosemann, R.; Cackovic, H. *J. Macromol. Sci. Phys.* **1974**, *B10*, 97.

(9) Wilke, W.; Gottlicher, K. *Colloid Polym. Sci.* **1981**, *259*, 596.

(10) Wilke, W. *Acta Crystallogr.* **1983**, *A39*, 864.

(11) Gottlicher, K.; Fronk, W.; Wilke, W. *Colloid Polym. Sci.* **1983**, *262*, 126.

(12) Fronk, W.; Wilke, W. *Colloid Polym. Sci.* **1985**, *263*, 97.

(13) Fronk, W.; Wilke, W. *J. Pol. Sci. Pol. Phys. Ed.* **1986**, *24*, 839.

(14) Wilke, W.; Bratrich, M. *J. Appl. Crystallogr.* **1991**, *24*, 645.

(15) Zheng, Z.; Nojima, S.; Yamane, T.; Ashida, T. *Polym. J.* **1989**, *21*, No. 1, 65.

(16) Zheng, Z.; Nojima, S.; Yamane, T.; Ashida, T. *Macromolecules* **1989**, *22*, 4362.

(17) Vonk, C. G.; *Colloid Polym. Sci.* **1979**, *257*, 1021.

(18) Vonk, C. G.; Kortleve, G. *Kolloid Z. Z. Polym.* **1967**, *220*, 19.

(19) Matsuo, M.; Kitayama, C. *Polym. J.* **1985**, *17*, No. 3, 479.

(20) Matsuo, M.; Sawatari, C. *Polym. J.* **1990**, *22*, No. 6, 518.

(21) Fu, Y.; Annis, B.; Boller, A.; Jin, Y.; Wunderlich, B. *J. Polym. Sci., Polym. Phys.* **1994**, *32*, 2289.

(22) Lee, K. G.; Schultz, J. M. *Polym.* **1993**, *34*, 4455.

(23) Rule, R. J.; Nye, T. M. W. *Nucl. Instrum. Methods B* **1995**, *97*, 248.

(24) Towns-Andrews, E.; Berry, A.; Bordas, J.; Mant, G.; Murray, P.; Roberts, K.; Sumner, I.; Worgan, J.; Lewis, R.; Gabriel, A. *Rev. Sci. Instrum.* **1989** *60* (7), 2346.

(25) Mahendrasingam, A.; Fuller, W.; Forsyth, V. T.; Oldman, R. J.; MacKerron, D. H.; Blundell, D. J. *Rev. Sci. Instrum.* **1992**, *63*, 1087.

(26) Fu, Y.; Busing, W. R.; Jin, Y.; Affholter, K. A.; Wunderlich, B. *Makromol. Chem.* **1994**, *195*, 803.

(27) Vonk, C. G.; Kortleve, G. *Koll. Z. Z. Polym.* **1967**, *220*, 19.

(28) Vonk, C. G. *J. Appl. Crystallogr.* **1971**, *4*, 340.

(29) Strobl, G. R.; Schneider, M. J.; *J. Polym. Sci., Polym. Phys. Ed.* **1980**, *18*, 1343.

(30) Jonas, A. M.; Russell, T. P.; Yoon, D. Y. *Colloid Polym. Sci.* **1994**, *272*, 1344.

MA9504173